MOTION ANALYSIS OF JUMP ROBOT WITH TETHER FOR LUNAR EXPLORATION

*Karin Kushida[1], Yuri Saito [2], Yoshiki Sugawara[3],

Sayako Sakama[4], Junichi Haruyama[5]

[1]*Aoyama Gakuin University, 5-10-1, Fuchinobe, Chuo-ku, Sagamihara-shi, Kanagawa-ken, Japan,*

E-mail: c5618133@aoyama.jp

[2]*Nagoya University, 464-8601, Furo-cho, Chikusa-ku, Nagoya, Japan,*

E-mail: saito.yuri@j.mbox.nagoya-u.ac.jp

[3] *Aoyama Gakuin University, 5-10-1, Fuchinobe, Chuo-ku, Sagamihara-shi, Kanagawa-ken, Japan,*

E-mail: sugawara@me.aoyama.ac.jp

[4] *Aoyama Gakuin University, 5-10-1, Fuchinobe, Chuo-ku, Sagamihara-shi, Kanagawa-ken, Japan,*

E-mail: sakama@me.aoyama.ac.jp

[5] *Institute of Space and Astronautical Science, Japan Aerospace Exploration Agency, 3-1-1, Yoshinodai, Chuo-ku, Sagamihara-shi, Kanagawa-ken, Japan, E-mail: haruyama.junichi@jaxa.jp*

ABSTRACT

On the moon, there are many terrains called "vertical holes" with larger depth-diameter ratio than that of normal craters. The hole has an overhanging part and a space like a cavity spreads under it. Then, it is also expected as a future candidate sites for underground resource exploration and lunar base, and so on. However, the hole or the cavity of the moon have not been explored yet. For the purpose of exploring them, the UZUME project (JAXA) is being advanced in Japan. In order to investigate them, it is supposed to put a mother machine in the vicinity of the hole entrance and explore inside of the hole and the cavity by another rover with an umbilical tether as a lifeline connected to the mother machine. In this study, in order to observe the side and bottom of the hole and cavity, a structure of a rover with tether is proposed. The proposed rover has function to descend or ascend within the hole stably and to travel on the bottom of the hole and cavity by wheel and jumping mechanism. Furthermore, in order to investigate the influence of the tether on jumping behavior of the rover, formulation of the rover with tether and numerical analyses for its jumping behavior are carried out.

1 INTRODUCTION

On the moon, there are many terrains called "vertical holes" with larger depth-diameter ratio than that of normal craters [1]. As shown in Fig.1, this terrain structure has an overhanging part included ground part, and a pot-shaped or tunnel-shaped space spreads under it. It is confirmed that the vertical hole at the Marius Hill (14.2 °N, 303 °E) has an underground cavity of about 50 km in length and its ceiling of the cavity has arched shape [2][3]. The wall of the vertical hole and the cavity are known to be composed of lava layers by imaging of Lunar Reconnaissance Orbiter (LRO) [4]. Because of high airtightness of the lava's feature, it is easy to make a pressurized space there and consequently it is possible to create a manned work space easily on the moon.

On the other hand, because the ceiling of the cavity is sufficiently thick for radiation protection, weathering by radiation is avoided, and sampling without weathering is expected. Because of above reasons, the vertical hole including the cavity is a research subject of the formation planetology, geology, life science, etc. of the rocky planet like Earth. Therefore, its importance has been drawing attention and it is expected as a candidate site for future lunar base development. However, no exploration of the vertical hole or the underground cavity of the moon is currently being carried out, and the internal environments are unknown.

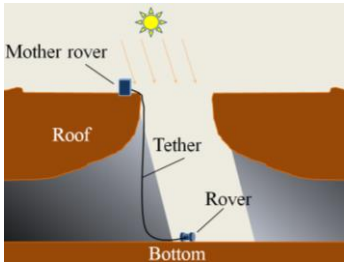

Figure 1: Mare Tranquillitatis Hole and overview of hole.

For the purpose of exploring the vertical hole and underground cavity of the moon, the project of

Unprecedented Zipangu Underworld of the Moon Exploration (UZUME) is being promoted mainly by JAXA in Japan [5]. Because it is an underground unknown environment there, it is supposed to put a mother machine in the vicinity of the hole entrance and explore the cavity by a rover with an umbilical tether as a lifeline as shown in Fig.1. Since it is observed that rubble is scattered on the bottom of the hole in range of the observation by orbiter [6], the rover is required to be equipped with a jumping mechanism aimed at getting over obstacles during traveling. In order to achieve running and jumping motion, two motors are installed and various investigations are going to be carried out by appropriately controlling them. However, the influence of the tether on the jumping behavior of the rover is not negligible, and it is necessary to analyze them and reflect the analysis results in design and operation of the rover. The mechanism with tether is used in many mechanical systems such as an underwater ROV (Remotely Operated Vehicle) [7], a tethered satellite [8], a wired drone [9], and so on. However, many studies on the motion of such mechanical systems deal with quasi-static motions, and there are very few studies attempting to analyze and control motion under dynamic conditions such as jumping of the rover with tether.

Since the tether is a quite flexible component, analysis considering large deformation is necessary in order to grasp the behavior of system with such a flexible component. In this study, Absolute Nodal Coordinate Formulation (ANCF) proposed by Shabana [10] et al. is employed as a formulation method of the tether part. ANCF is a kind of nonlinear finite element method. In the formulation by ANCF, displacements and gradients of nodes represented by absolute coordinate system are introduced as nodal coordinates, and consequently ANCF can accurately represent various kinds of motion and deformation with fewer elements than the conventional finite element method. Therefore, the aim of this study is to propose a mechanical system required for the aforementioned mission, to derive the mathematical expression of the proposed jumping rover with tether by use of ANCF and concept of multibody dynamics, and furthermore to grasp its behavioral characteristics by numerical analyses.

This paper is organized as follows. In Section 2, required mission for the rover is defined and the structure of the rover associated with the mission is introduced. Then, mathematical expressions for the rover are derived in Section 3. In Section 4, numerical analyses are carried out by use of the mathematical expression derived in the previous section and discussions on the design and operation of the rover are done on the basis of the obtained results of numerical analyses. Finally, conclusions and future works are described in Section 5.

2 OPERATION SEQUENCE AND CONFIGURATION OF THE ROVER

The rover separated from the mother machine descends by use of tether into the vertical hole and lands on the bottom of the vertical hole. When the rover is descending, it observes the side of the vertical hole and inside of the cavity. And then, after the landing on the bottom, various observations are executed by the rover at the bottom of the hole and the cavity. Furthermore, after the end of the observation at the bottom, the rover is pulled up by the mother machine, and again observes the sides of the vertical hole and the cavity while being pulled up. To summarize the above sequences, the operation sequence of the rover can be classified into two phases as Fig.2 shows. One is the "Phase (A)" where the observations of the side of the vertical hole and cavity are carried out by the rover when it is descending or ascending within the vertical hole. The other is "Phase (B)" where investigations of the bottom of the vertical hole and the cavity are done by the rover.

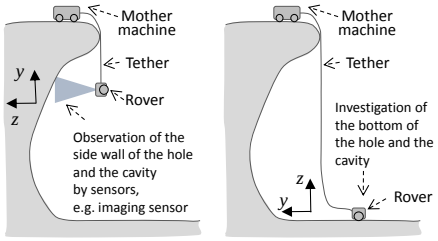

Figure 2: Two phases in the operation of the rover. (Left: Phase (A), Right: Phase (B))

In the Phase (A), oscillation of the rover might occur because it hangs from the mother machine by a tether. Therefore, for example, observation by an image sensor will receive an influence from such an oscillation. Therefore, it is necessary to suppress such an oscillation and control rover's attitude by installing some actuators for control. On the other hand, in the Phase (B), traveling mechanism has to be installed to achieve locomotion in the bottom of the hole and the cavity. In addition to traveling mechanism, jumping mechanism is also required in order to escape from stack state of the rover because it is known that debris is scattered in the bottom as mentioned before. However, if actuators are mounted so as to satisfy each requirement for both phases mentioned above, the system may become complicated and the reliability of the entire system may be deteriorated. Therefore, in this study, a system as shown in Fig.3 is proposed. Fig.3 shows only the systems related to the mechanical system required for two phases described above, and the other systems, e.g. power system communication system and so on, are not depicted for the sake of

clear illustration of the proposed system. The mechanical part in Fig.3 can be roughly divided into two parts. One is a traveling mechanism by a wheel and the other is a mechanical system for jumping. Fig. 4 shows the traveling mechanism by wheels. This mechanism has a mechanism like a differential gear. Installing bevel gears and ratchet mechanisms on each wheel drive system, straight and swirling motion can be achieved by combination of positive and inverse rotation of one motor.

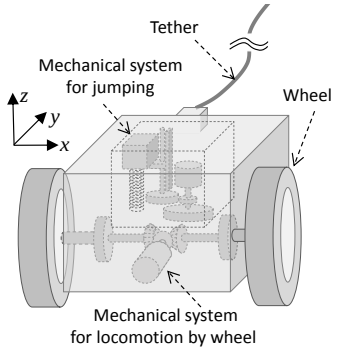

Figure 3: Simplified schematic of the proposed rover.

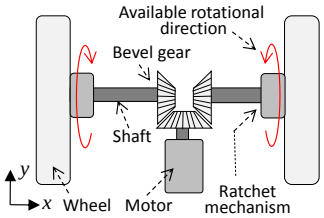

Figure 4: Traveling mechanism by wheels

Fig. 5 shows mechanical system for jumping. The mechanism mainly consists of one motor, a ball screw, a slider, a mass (Body 2 to be described later), a latch mechanism, a gear, a spring, and a wheel. Rotating the axis of the motor in the appropriate direction, the translation parts of the ball screw pushes Body 2 in the -*z* direction through the latch, whereby the spring is compressed and the potential energy of the spring is stored. As the spring is further pushed in, as shown in Fig. 6, the latch mechanism installed on Body 2 moves to the leftward and the Body 2 has a velocity upward by the spring at the moment of the release of the latch mechanism, and that leads to the jump of the rover. As shown in Fig. 7, when the spring is fully extended, the translation parts of the ball screw is moved upward by the appropriate rotation of the motor, and the translation parts of the ball screw can hook the latch installed in the Body 2, and then the spring is ready to be compressed again.

On the other hand, because torque can be generated in the rotation direction of the wheel by the motor drive system, it becomes possible to control the attitude of the rover around the *x* axis in the Phase (A). In addition, as shown in Fig. 5, a wheel is installed on the motor shaft of the jumping mechanism, and it is possible to use the mechanism for jumping as a function of the reaction wheel in a state where the translational movement part of the ball screw is not in contact with Body 2. As a result, it is possible to realize the attitude control of the rover around the y axis of the Phase (A) as shown in Fig. 2. By properly performing control around the y axis, it is also possible to rotate the rover around the tether and to control the attitude around the z axis in Phase (A).

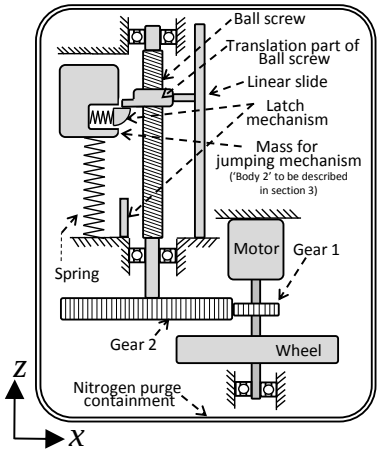

Figure 5: Mechanical system for jumping

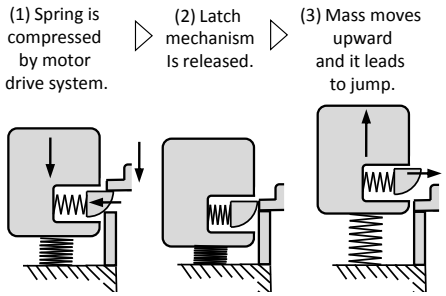

Figure 6: Release of latch mechanism.

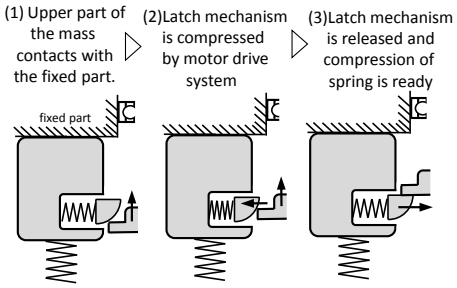

Figure 7: Hooking of latch mechanism.

As described above, by utilizing the mechanical system designed for the operation in Phase (B), the proposed system can control the attitude of the rover in Phase (A). In other words, actuators installed for Phase (B) can be used as reaction wheel for control of the rover in Phase (A). Note that it is considered that a highly reliable system can be achieved since the number of motor installed in the proposed system is only two. However, further consideration for detail specification remains and additional improvement has to solve the drawback that the angular momentum

which can be absorbed by the reaction wheel is reduced by frictional forces due to the introduction of gears and ball screws.

3 ANALYSIS OBJECT AND FORMULATION OF THE OBJECT

3.1 Analysis Object

In this study, in order to reveal the fundamental characteristic of the jumping motion of the rover with tether, a simplified model is introduced in Fig. 8 as an analysis target, which moves on a two-dimensional plane. In order to consider essential jumping function of the rover, two rigid bodies connected by a slider joint represent the rover, and the lower part is defined as Body 1 and the upper part is defined as Body 2. Furthermore, the rigid bodies have uniform mass density, spring is attached between two bodies for the jumping mechanism, and damper is also implemented in parallel with the spring in order to represent the internal viscosity of the mechanism. One end of the tether is attached to the Body 1, and the other end is attached to the inertial frame which is assumed to be the mother machine. Furthermore, the tether has uniform material density and uniform cross-sectional shape. In the following sections, mathematical expression is derived for the above simple model.

3.2 Formulation of the Tether by ANCF

In order to formulate the tether by Absolute Nodal Coordinate Formulation (ANCF), the tether is assumed to be very flexible planar beam and is divided into n beam elements. Then, ANCF is applied to each beam element. As shown in Fig. 9, global coordinate vector of an arbitrary point P on the neutral axis of i-th beam element is expressed as follows [11].

$$\mathbf{r}_i = \mathbf{S}_i(x_i)\mathbf{e}_i \tag{1}$$

where $\mathbf{S}_i(x_i)$ is shape function matrix, x_i is local coordinate of the non-deformed element, and $\mathbf{e}_i$ is nodal coordinate vector. Displacements and gradients of both nodes are used as nodal coordinates and definitions of each component of $\mathbf{e}_i$ is given by

$$\mathbf{e}_i = [e_{i1} \quad e_{i2} \quad \cdots \quad e_{i8}]^T \tag{2}$$

$$\begin{aligned} &e_{i1} = X_i\big|_{x_i=0}, e_{i2} = Y_i\big|_{x_i=0}, e_{i3} = \left.\frac{\partial X_i}{\partial x_i}\right|_{x_i=0}, e_{i4} = \left.\frac{\partial Y_i}{\partial x_i}\right|_{x_i=0} \\ &e_{i5} = X_i\big|_{x_i=l_i}, e_{i6} = Y_i\big|_{x_i=l_i}, e_{i7} = \left.\frac{\partial X_i}{\partial x_i}\right|_{x_i=l_i}, e_{i8} = \left.\frac{\partial Y_i}{\partial x_i}\right|_{x_i=l_i} \end{aligned} \tag{3}$$

where l_i is the length of non-deformed i-th beam element. By use of the aforementioned definition of nodal coordinate vector, the kinetic energy of the i-th element is given as follows.

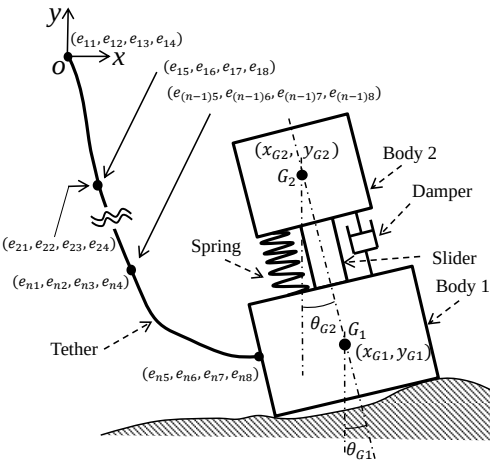

Figure 8: Simplified model for formulation.

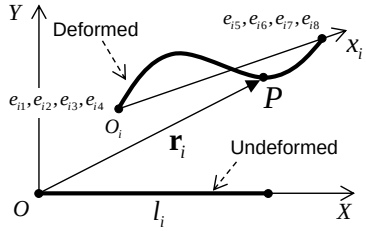

Figure 9: The i-th beam element by ANCF.

$$\begin{aligned} T_i &= \frac{1}{2}\int_V \rho \dot{\mathbf{r}}_i^T \dot{\mathbf{r}}_i \, dV = \frac{1}{2}\int_V \rho \dot{\mathbf{e}}_i^T \mathbf{S}_i^T \mathbf{S}_i \dot{\mathbf{e}}_i \, dV \\ &= \frac{1}{2}\dot{\mathbf{e}}_i^T \mathbf{M}_i \dot{\mathbf{e}}_i \end{aligned} \tag{4}$$

Note that inertia matrix $\mathbf{M}_i$ is constant matrix, consequently Coriolis and centrifugal force are equal to zero, which is one of the feature of the formulation by ANCF.

Bending strain energy of the i-th beam element is given as follows:

$$U_{it} = \frac{1}{2}\int_0^{l_i} E_i I_i \kappa_i^2 \, dx_i \tag{5}$$

where U_{it}, E_i, I_i, κ_i are bending strain energy, Young's modulus, the geometrical moment of inertia and the curvature, respectively. The bending elastic force vector $\mathbf{Q}_{it}$ is derived by differentiating U_{it} with respect to $\mathbf{e}_i$. Then, $\mathbf{Q}_{it}$ is expressed by the product of the bending stiffness matrix and the absolute nodal coordinate vector such as the following equation:

$$\mathbf{Q}_{it} = \left(\partial U_{it}/\partial \mathbf{e}_i\right)^T = \mathbf{K}_{it}(\mathbf{e}_i)\mathbf{e}_i \tag{6}$$

where $\mathbf{K}_{it}$ is a bending stiffness matrix. Employing T1 model proposed by Berzeri et.al.[11], which is used when the longitudinal deformation is small, bending stiffness matrix $\mathbf{K}_{it}$ becomes constant matrix.

The longitudinal strain energy of the i-th beam element is given as follows:

$$U_{it} = \frac{1}{2}\int_0^{l_i} E_i A_i \varepsilon_i^2 \, dx_i \tag{7}$$

where U_{il}, A_i, ε_i are longitudinal strain energy, cross sectional area and axial strain of the i-th beam element, respectively. Introducing the Green-Lagrange stain and differentiating the longitudinal strain energy with respect to nodal coordinate vector given by Eq.(2), force vector by longitudinal deformation $\mathbf{Q}_{il}$ is given by

$$\mathbf{Q}_{il} = \left(\partial U_{il}/\partial \mathbf{e}_i\right)^T = \mathbf{K}_{il}\left(\mathbf{e}_i\right)\mathbf{e}_i \tag{8}$$

where $\mathbf{K}_{il}$ ($\mathbf{e}_i$) is stiffness matrix associated with longitudinal deformation and note that the matrix depends on the nodal coordinate and consequently stiffness term shows nonlinearity. Depending on the definition of longitudinal strain, there are several models of $\mathbf{K}_{il}$ ($\mathbf{e}_i$) and L2 model proposed by Berzeri et.al. [11] is employed in this study.

Applying Lagrange equation to the energy given by Eq.(4), (5) and (7) and considering the relations given by Eq. (6) and (8), equation of motion for i-th element is derived as follows:

$$\mathbf{M}_i \ddot{\mathbf{e}}_i + \mathbf{K}_{it}\,\mathbf{e}_i + \mathbf{K}_{il}\left(\mathbf{e}_i\right)\mathbf{e}_i = \mathbf{Q}_i \tag{9}$$

where $\mathbf{Q}_i$ is external force vector.

3.3 Formulation of Jumping Rover

In order to apply the concept of multibody dynamics to formulation of the jumping rover, generalized coordinates vector $\mathbf{G}_1$ and $\mathbf{G}_2$ are defined for Body 1 and 2 of the rover's main body as

$$\mathbf{G}_1 = [x_{G1} \quad y_{G1} \quad \theta_{G1}]^T, \mathbf{G}_2 = [x_{G2} \quad y_{G2} \quad \theta_{G2}]^T \tag{10}$$

where x_{G1}, y_{G1}, θ_{G1}, x_{G2}, y_{G2} and θ_{G2} are components of $\mathbf{G}_1$ and $\mathbf{G}_2$ as shown in Fig. 8.

Then, equations of motion for Body 1 and 2 are expressed as

$$\begin{cases} m_1 \ddot{x}_1 = f_{1x} \\ m_1 \ddot{y}_1 = f_{1y} \\ m_1 \ddot{\theta}_1 = \tau_{1x} \end{cases} \tag{11}$$

$$\begin{cases} m_2 \ddot{x}_2 = f_{2x} \\ m_2 \ddot{y}_2 = f_{2y} \\ m_2 \ddot{\theta}_2 = \tau_{2y} \end{cases} \tag{12}$$

where m_i (i=1,2) represents mass of Body i, f_{ix} and f_{iy} are forces in the direction of x and y and τ_i (i=1,2) is torque applied to Body i.

For the sake of the jumping mechanism, Body 1 and 2 are constrained as to move in one direction relatively and spring is installed between Body 1 and 2. Then, constraint equation $\mathbf{C}_b$ is derived to expresses constraints on the translation and rotation between Body 1 and 2 as

$$\mathbf{C}_b = \begin{bmatrix} C_{b1} \\ C_{b1} \end{bmatrix} = \begin{bmatrix} -\cos\theta_{G1}(x_{G2} - x_{G1}) - \sin\theta_{G1}(x_{G2} - x_{G1}) \\ \sin(\theta_{G2} - \theta_{G1}) \end{bmatrix} = \mathbf{0} \tag{13}$$

Furthermore, the product of the translational force by the spring between the centers of gravity of Body 1 and 2 is derived by virtual work principle. The generalized force F is derived as

$$F = k\left(l\left(\mathbf{G}_1, \mathbf{G}_2\right) - l_0\right) \tag{14}$$

where k is spring constant, l_0 is natural length of the spring and l is the relative distance between Body 1 and 2 which depends on $\mathbf{G}_1$ and $\mathbf{G}_2$. The derived force F is applied to each body as forces given in Eq. (11) and (12).

3.4 Derivation of Differential Algebraic Equation

In order to derive the motion of equation for whole system, constraint relations of composing elements have to be described, that is, constraints between tether and ground, constraints between intermediate beam elements and constraints between tether and jumping rover.

First is the constraints between tether and ground. One end of the tether is fixed to ground and it is assumed that one end of the first element of the beam is fixed by pinned support to the origin of a frame fixed to the ground. Such constraints are given by

$$\begin{bmatrix} C_{gt1} \\ C_{gt2} \end{bmatrix} = \begin{bmatrix} e_{11} \\ e_{12} \end{bmatrix} = \mathbf{0} \tag{15}$$

Next is the constraints between intermediate beam elements. Neighboring intermediate elements are connected to each other so that the displacements and gradients of both connected nodes have same values. Then, constraint on the connection of element i and i+1 are expressed by

$$\begin{bmatrix} C_{ti(i+1)1} \\ C_{ti(i+1)2} \\ C_{ti(i+1)3} \\ C_{ti(i+1)4} \end{bmatrix} = \begin{bmatrix} e_{i5} - e_{(i+1)1} \\ e_{i6} - e_{(i+1)2} \\ e_{i7} - e_{(i+1)3} \\ e_{i8} - e_{(i+1)4} \end{bmatrix} = \mathbf{0} \tag{16}$$

where i=1,2, … n-1.

The last remaining constraint is that between tether and jumping rover. The other end of the tether is fixed to the Body 1 of the rover by pinned support and the constraints are given by

$$\begin{bmatrix} C_{tr1} \\ C_{tr2} \end{bmatrix} = \begin{bmatrix} e_{n5} - X_{G1} + \sqrt{a^2 + b^2}\cos\left(\frac{\pi}{2} - \left(\theta_{G1} + a\tan\frac{b}{a}\right)\right) \\ e_{n6} - Y_{G1} + \sqrt{a^2 + b^2}\sin\left(\frac{\pi}{2} - \left(\theta_{G1} + a\tan\frac{b}{a}\right)\right) \end{bmatrix} = \mathbf{0} \tag{17}$$

where n is the number of elements of the tether, a and b are the parameter which defines the tether connecting position on the Body 1 as shown in Fig. 8.

Based on the concept of multibody dynamics and using above constraint equations, the equation of motion is expressed as differential algebraic equation (DAE):

$$\begin{bmatrix} \mathbf{M} & \mathbf{C}_\mathbf{q}^{\mathrm{T}} \\ \mathbf{C}_\mathbf{q} & \mathbf{0} \end{bmatrix} \begin{bmatrix} \ddot{\mathbf{q}} \\ \boldsymbol{\lambda} \end{bmatrix} = \begin{bmatrix} \mathbf{Q}_E \\ \boldsymbol{\gamma} \end{bmatrix} \tag{18}$$

where $\mathbf{M}$ is mass matrix which consists of $\mathbf{M}_i$ (i=1,2, $\cdots$,n), m_1 and m_2. $\mathbf{C}_\mathrm{q}$ is the Jacobian obtained from the constraint equation vector $\mathbf{C}$ which consists of constraint equations derived above, $\boldsymbol{\gamma}$ is the term related to acceleration derived from differentiation of constraint equation, $\boldsymbol{\lambda}$ is undetermined multiplier vector, and $\mathbf{Q}_\mathrm{E}$ is the external force vector including the force due to the stiffness of the tether.

Here, in order to avoid the singular state caused by numerical analysis, the divergence is suppressed by adopting the damping term in the constraint equation as shown in Eq. (19).

$$\mathbf{C} + \upsilon \dot{\mathbf{C}} = \mathbf{0} \tag{19}$$

where υ is a positive arbitrary constant.

Using Eq. (19), equation of motion in DAE form is newly derived as a DAE given by Eq. (20).

$$\begin{bmatrix} \mathbf{M} & -\upsilon\mathbf{C}_\mathbf{q}^{\mathrm{T}} \\ \mathbf{C}_\mathbf{q} & \mathbf{0} \end{bmatrix} \begin{bmatrix} \ddot{\mathbf{q}} \\ \dot{\tilde{\boldsymbol{\lambda}}} \end{bmatrix} = \begin{bmatrix} \mathbf{Q}_\mathrm{E} - \mathbf{C}_\mathbf{q}^{\mathrm{T}}\tilde{\boldsymbol{\lambda}} \\ \boldsymbol{\gamma} \end{bmatrix} \tag{20}$$

where $\tilde{\boldsymbol{\lambda}}$ is new undetermined multiplier vector for the sake of introduction of Eq. (19).

4 NUMERICAL ANALYSIS

4.1 Numerical Analysis on Influence of Tether Stiffness

It is expected that stiffness of the tether would have influence on the jumping behavior of the rover. But the influence of the stiffness may be different depending on the shape of the tether. Therefore, "Slack evaluation value" is introduced to evaluate the shape of the tether in this study. Here, the slack evaluation value is defined as a ratio between vertical and horizontal distance from the tether starting position to the rover connecting position as shown in Fig. 10, that is *Δh/Δf*. For different slack evaluation values, rover's jumping height and variation of attitude angle between initial angle and landing angle are compared by numerical analysis based on the obtained mathematical model derived in the previous section. Such an analysis is done for different stiffness of the tether, and the influence of the stiffness on the behavior is investigated. Table 1 shows the analysis conditions, and Fig. 11 and 12 show the analysis results. In the numerical analyses, numerical analyses starts from the moment when the rover has the initial velocity for jumping in order to eliminate the influence of the ground.

As shown in Table 1, two different Young's modulus are introduced for two cases, i.e. low and high stiffness of the tether, and the others are common parameters. It can be seen from Fig. 11 and 12 that when the Young's modulus is low, the behavior of the rover is not influenced by the slack state of the tether. On the other hand, when the Young's modulus is high, the attitude largely varies depending on the slack state of the tether. Regarding the jumping height, when the Young's modulus is low, it seems that there is no correlation with the slack state, but when the Young's modulus is high, there is a large variation with respect to the slack evaluation value, and it was confirmed that the initial state of the tether have significant influence on the jumping height. Such obtained results are useful when the rover is operated. Suppose that high stiffness of the tether can not be avoided due to design requirement, then slack state of the tether is used for prediction of the jumping behavior. For example, if slack evaluation value is high, higher jump may lead to large variation of landing attitude, then smaller jump is chosen in order to avoid the undesirable attitude for equipped component, e.g. solar cell, communication antenna and so on.

Table 1. Parameters for analyses

Young's modulus E (low) [GPa]	0.01
Young's modulus E (high) [GPa]	0.5
Element number of tether N_i	5
Length l [m]	5
Radius r [m]	3.45×10^{4}
Density ρ [kg / m^3]	1.00×10^{4}
Acceleration of gravity g [m / s^2]	9.81
Mass of Body1 m_1 [kg]	3.0
Mass of Body2 m_2 [kg]	2.0
Spring constant k [N/m]	824

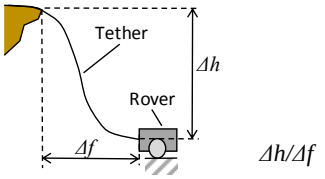

Figure 10: Definition of slack evaluation value.

4.2 Numerical analysis on body mass

In this section, influence of the mass of Body 2, which is a component of jumping mechanism, is investigated. As in the previous section, numerical analyses are carried out in order to derive the jumping height and attitude variation for different slack evaluation values and such numerical analyses are carried out for different masses of Body 2. Table 2 shows analysis conditions, and analyses are carried out for two cases. Case 1 and 2 are the cases of heavy and light mass of Body 2, respectively. Fig. 13 and 14 show the jumping height and variation of attitude

angle of the body for case 1 and 2, respectively. As shown in Fig. 13, it can be seen that the jumping height increases extremely when the slack evaluation value is more than 1.5. Therefore, as an example of operational strategy, it is possible to employ a method as to operate the rover in the range where higher jumping height is achieved for effective operation, that is in the range where the evaluation value becomes more than 1.5. By use of such an operation method, it is possible for the rover to avoid obstacles efficiently. When the slack evaluation value is less than 1.5, the attitude variation amount is small, whereas, the attitude variation amount takes various values when the evaluation value is more than 1.5. This is due to the fact that when the slack evaluation value is small, the jumping amount becomes small. Consequently, the duration in which the attitude variation continues is short and the rover would land immediately without large variation of the attitude.

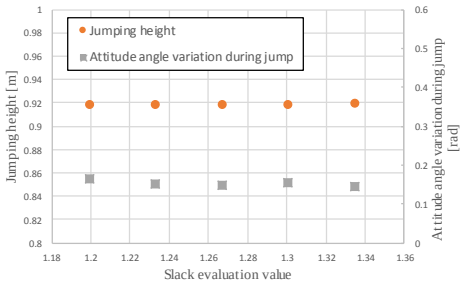

Figure 11: Analysis result (low young's modulus).

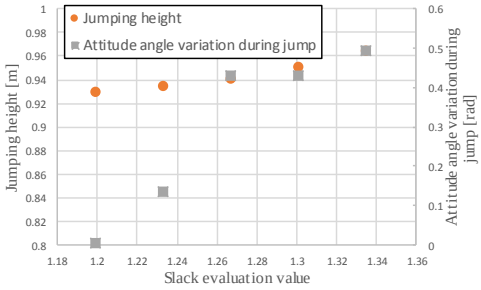

Figure 12: Analysis result (high young's modulus).

On the other hand, as shown in Fig.14, both the jumping height and the variation amount of attitude angle change less than those of the case 1. From these results, it can be seen that the mass of body 2 has a large influence on the jumping height and attitude angle variation.

Table 2. Analysis conditions

Length l [m]	5
Radius r [m]	3.45×10^4
Density ρ [kg / m^3]	2700
Young's modulus E [GPa]	70
Initial position θ_0 [deg]	10
Mass of Body1 m_1 [kg]	10
Mass of Body2 for case1 m_2 [kg]	0.5
Mass of Body2 for case2 m_2 [kg]	0.05

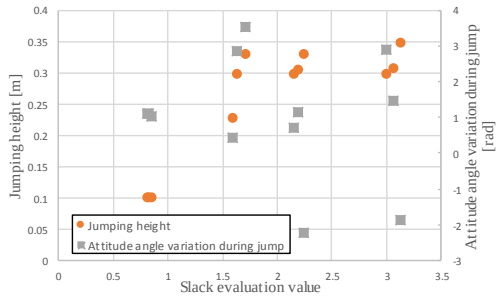

Figure 13: Analysis results of case 1.

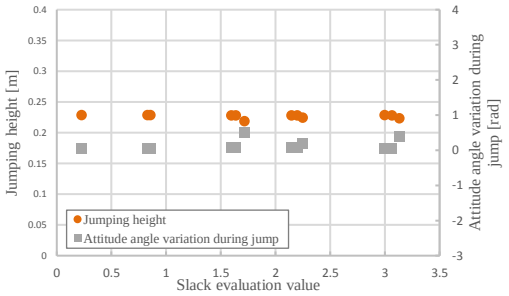

Figure 14: Analysis results of case 2.

In general, the rover has limits on its total mass in a practical sense. Therefore, the total mass is supposed to be constant and numerical analyses are done for different mass ratio. The characteristics of jumping behavior of the rover are examined in numerical analyses by comparing the results for different mass ratios. In the analyses, the total mass value is set to be 10.05 kg, and other parameters have same values with those of Table 2. A comparison of jumping heights is shown in Fig. 15.

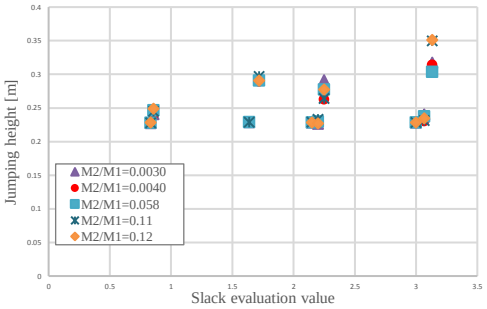

Figure 15: Jumping height with respect to different slack evaluation value for difference mass ratios.

It is recognized from Fig. 15 that there is no large difference in the jumping height for different mass ratio. This result suggests that the jumping height is not be affected by the tether and potential energy of the spring is converted to the jumping height without large influence of the tether. However, it is observed that the larger slack evaluation value, e.g. when slack evaluation value is about 3.1, leads to larger difference of the jumping height compared to others.

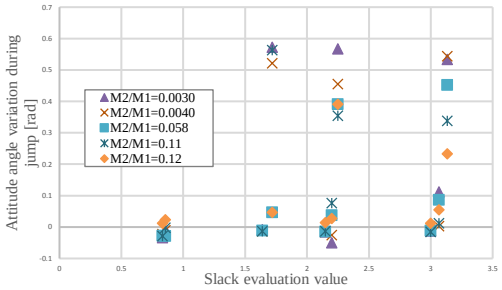

Figure 16: Attitude angle variation with respect to different slack evaluation value for difference mass ratios.

Fig.16 shows attitude angle variation during jump of the rover for different mass ratios. As these results show, the larger the mass ratio is, the more the angle variation during jump tends to change due to a slight change in the mass ratio. On the other hand, when the mass ratio is relatively small, the amount of angle variation hardly changes due to the change in the mass ratio, and the values converge. In other word, slack evaluation value has larger influence on the attitude angle variation when slack evaluation value is large, i.e. the value is larger than 1.5 in this case.

Above characteristics are available on operation. For example, for the purpose of stable and effective operation of the rover, jumping mechanism is used for locomotion when the slack evaluation value is small and wheel mechanism is used for locomotion when the slack evaluation value is small. By such an operation strategy, the rover can avoid the unexpected rollover while effective locomotion is achieved by applying jumping locomotion.

5 CONCLUSION AND FUTURE WORKS

Focusing on the wheel traveling function and the jumping function of a rover with a tether, a mechanical structure was proposed. Furthermore, DAE was derived for the rover with tether in order to investigate its jumping behavior. By use of the obtained DAE, numerical analyses were performed to derive the attitude variation angles and jumping heights for different slack evaluation values. Numerical analyses revealed the dependency of some parameters on the jumping height and attitude angle variation. Furthermore, according to the obtained results, some examples for design and operation strategy of the rover were given.

As a future work, the results of numerical analyses should be validated by experiments. Furthermore, in order to discuss more practical feature of the rover, equation of motion for 3-dimensional model of rover are also required and formulation of wheel and ground on which the rover travel is quite important for more detail analysis. Then, obtained results would be applied to the development of the rover.

References

[1] Haruyama J, Hioki K, Shirao M, Morota T, Harald H, Carolyn H, Miyamoto H, Iwasaki A, Yokota Y, Ohtake M, Matsunaga T, Hara S, Nakanotani S and Carle M (2009) Possible lunar lava tube skylight observed by SELENE cameras. Geophysical Research Letters, Vol.36, p.L21206.

[2] Loic C, Rohan S, Henry J, Kathleen C, David M, Colleen M and Maria T (2016) Evidence of large empty lava tubes on the Moon using GRAIL gravity. Geophysical Research Letters, Vol.44, pp.105-112.

[3] Kaku T and Haruyama J (2017) Detection of intact lava tubes at Marius Hills on the Moon by SELENE (Kaguya) Lunar Radar Sounder. Geophysical Research Letters, pp.10155-10161.

[4] Bowker D, and Hughes J (1971) Lunar Orbiter photographic atlas of the Moon. NASA Spec. Publ., NASA SP‐206.

[5] Haruyama J and Kawano I (2014) Unprecedented Zipangu Underworld of the Moon Exploration (UZUME). Proceeding of European Planetary Science Congress 2014, Vol. 9, pp.465-466.

[6] Sugawara Y, Mizuguchi K, Kobayashi N (2010) A hopping mechanism through the use of resonance (an analytical study and proposal for an effective hopping method). Journal of System Design and Dynamics, Volume 4, Issue 1, pp.115-128.

[7] Burgess J (1994) The deployment of an undersea cable system in sheared current. Proceedings of BOSS'94, p. 327–334

[8] Kawamoto S and Kikkawa C (2010) Control technologies required for electrodynamic tethers and active debris removal. Transactions of the Japan Society for Aeronautical and Space Science, Aerospace Technology Japan, Vol.8, ists27, pp. To_4_1To_4_6.

[9] Marco M, Roberto N and Emanuele G (2014) Taut cable control of a Tethered UAV. IFAC Proceedings Volumes, Vol.47, Issue 3, pp.3190-3195.

[10] Escalona J, Hussien H and Shabana A (1998) Application of the Absolute Nodal Co-Ordinate Formulation to multibody system dynamics. Journal of Sound and Vibration, Volume 214, Issue 5, 30 July, pp.833-851.

[11] Berzeri M and Shabana A (2000) Development of simple models for the elastic forces in the absolute nodal co-ordinate formulation. J. Sound Vib. 235(4), pp.539–565.